Multiplication noise in the human visual system at threshold: 1. Quantum fluctuations and minimum detectable energy

Malvin Carl Teich, Paul R. Prucnal, Giovanni Vannucci,*

Michael E. Breton,† and William J. McGill‡

Columbia University, New York, New York 10027

Received June 11, 1981; revised manuscript received November 17, 1981

We have carried out a series of frequency-of-seeing experiments similar to those performed by Hecht, Shlaer, and Pirenne [J. Gen. Physiol. **25**, 819–840 (1942)], using an Ar^+ laser operated at 514.5 nm as the source of light. In certain blocks of trials, our subjects were encouraged to report as seen those trials in which the stimulus might have been present. It was determined that sensitivity and reliability were traded against each other over a broad range: for our four subjects, the detection of 147 photons at the cornea with 60% frequency of seeing entailed, on the average, a 1% false-positive rate (FPR), whereas the detection of 34 photons at the cornea with 60% frequency of seeing was accompanied by a 33% FPR. A new neural-counting model has been developed in the framework of signal-detection theory. It combines Poisson stimulus fluctuations with additive and multiplicative neural noise, both of which are known to be present in the visual system at threshold. The resulting probability-of-detection curves, derived from the Neyman Type-A counting distribution, are in good accord with our experimental frequency-of-seeing data for sensible values of the model parameters. We deduce that, on the average, our four subjects are able to detect a single photon at the retina with 60% frequency of seeing, at the expense of a 55% FPR. In Part 2 of this set of papers [P. R. Prucnal and M. C. Teich, Biol. Cybern. **43**, 87–96 (1982)], we use the normalizing transform, together with probit analysis, to provide improved estimates of threshold parameters, whereas in Part 3 [M. C. Teich, P. R. Prucnal, G. Vannucci, M. E. Breton, and W. J. McGill, submitted to Biol. Cybern.], we consider the effects of non-Poisson quantum fluctuations.

1. INTRODUCTION

The classic experiment of Hecht, Shlaer, and Pirenne[1] (HSP), carried out at Columbia University in 1942, needs little introduction to an audience of visual scientists. Although the first measurement of the minimum light energy required to elicit a response from the human visual system was made by Langley some 50 years earlier,[2] HSP conducted their experiments under optimal conditions for seeing and approached the problem in two distinct ways. On the one hand, they performed a straightforward photometric measurement of the average number of photons required at the cornea for 60% frequency of seeing. They concluded that this number lay between 54 and 148 quanta for their seven subjects, corresponding to a range of 5–14 quanta at the retina, after accounting for estimated losses as best as they were known in 1942. On the other hand, they created a simple model for retinal response based on the Poisson statistical fluctuations of the small numbers of photons expected to be absorbed there. This led them to conclude, from an independent measurement of the shape of the frequency-of-seeing curve, that the number of photons absorbed by the retina lay between five and eight. This close agreement has served to support the validity of their model, and the notions introduced by HSP have pervaded visual theory ever since. It is important to note, however, that the actual number of photons absorbed by the retina has never been directly determined.

At about the same time, on the other side of the Atlantic, similar experiments were reported by van der Velden.[3] Many different hypotheses were developed by various researchers in an attempt to explain the frequency-of-seeing results and to tie them to related measurements. The two-quantum hypothesis was set forth by van der Velden[3] and studied by Bouman and van der Velden[4] and Baumgardt.[5] Blackwell[6] developed a comprehensive theory related to Crozier's[7] early neural hypothesis.

A number of researchers considered the importance of various kinds of additive noise in limiting visual-system performance,[8,9] and signal-detection theory (SDT) was applied to these problems.[10–16] Multiple-channel models[15,17] were presented by Nachmias and Kocher[18] and by Cohn *et al.*,[19] who incorporated into their SDT models the additional effects of channel uncertainty and location/temporal uncertainty, respectively. Some workers in the field[15,18,20,21] introduced the use of rating-scale (viz., M-ary detection and estimation[16]) formats in their experiments in place of the yes–no (nonorthogonal binary) format used by HSP. A number of review articles detailing most of these efforts have been written over the years.[22–26]

Most closely related to our approach, however, are the quantitative models for threshold visual detection proposed by Barlow[27] in 1956 and by McGill[28,29] in 1967. Both are based on Poisson stimulus fluctuations and SDT, but the character of the noise is assumed to be different in each. In Barlow's model, the Poisson noise is considered to arise peripherally and to be additive, whereas in McGill's model it is considered to arise centrally and to be multiplicative. In 1977, Barlow[30] also discussed the importance of including the effects of central noise in dealing with threshold detection. The model that we develop here incorporates both of these sources of noise. It combines Poisson stimulus fluctuations, additive Poisson noise, and multiplicative Poisson noise, all of which are known to be present in the visual system at threshold, in

0030-3941/82/040419-13$01.00

an SDT framework. It has been designed to be consistent with the character of the neural noise that is measured physiologically at various stations along the optic pathway.

We have conducted a series of frequency-of-seeing experiments, similar to those performed by HSP, using an Ar^+ laser operated at 514.5 nm as the source of light. In certain blocks of trials, we encouraged our subjects to report as seen those trials in which the stimulus might have been present, without regard to the possibility of reporting a false positive. We thereby obtained sets of experimental data with greatly varying false-positive rates, enabling us to demonstrate that the model parameters extracted from our data are physiologically sensible.

In Section 2, we describe the experimental setup and paradigm. The results of our experiments are provided in Section 3, in which we present frequency-of-seeing curves obtained under conditions of varying reliability of response, which is a critical determinant of the average number of quanta required at the cornea for 60% seeing. Sources of noise arising from stimulus fluctuations, and from additive and multiplicative noise in the visual system, are described in Section 4. This permits us to frame a plausible model for threshold visual detection that treats these fluctuations in conjunction with a decision strategy based on SDT. The development presented in Section 4, in turn, allows us to extract estimates for various model-dependent physiological parameters from our frequency-of-seeing data (e.g., the average number of photons absorbed at the retina), and we carry this out in Section 5. The conclusion is presented in Section 6.

In Part 2 of this set of papers,[31] we use the normalizing transform, and probit analysis, to provide improved estimates of threshold parameters. In Part 3,[32] we consider quantum fluctuations for non-Poisson stimuli. A preliminary report of our experimental results was presented in abstract form in 1979.[33]

2. EXPERIMENT

A. Equipment

An abbreviated schematic representation of the experimental apparatus used to generate stimuli and to record and tabulate responses is presented in Fig. 1. With the left eye, the subject viewed a small, dim, red fixation target produced by a Maxwellian system (not shown). The 5′ disk-shaped light stimulus, presented at 17.5° horizontal eccentricity on the temporal retina, was produced by a laser that was viewed directly (see lower portion of figure). The source was a feedback-stabilized Spectra-Physics Model 162 Ar^+ ion laser, which produced plane-polarized radiation at 514.5 nm, in the blue-green region of the spectrum, by oscillation on several longitudinal modes.[34] The light was attenuated by using neutral-density filters (not shown) before it entered the subject's eye. A sheet polarizer was the final element in the optical path to ensure that the stimulus sent to the subject was plane polarized.

The light intensity was controlled by an acousto-optic modulator driven by the system shown in the upper portion of Fig. 1. A signal generator produced a continuous triangular wave with a frequency of 2 Hz. When the subject pressed the start-trial switch, a rectangular pulse with a duration of 1 msec was added to the triangular wave in such a way that the threshold necessary to turn the light modulator control on was exceeded. By selecting the amplitude and dc bias of the triangular wave and the pulse height, various modulation depths (M) and average light intensities could be generated. In the experiments reported in this paper, M was set equal to zero so that the acousto-optic device passed 1-msec pulses of unmodulated laser light of adjustable average energy. Experiments in which M was not equal to zero are reported in Part 3 of this series of papers.[32]

Part of the light output from the laser was removed by a beam splitter and detected by a silicon photocell (see lower portion of figure). The photocell output formed the input to a feedback circuit that stabilized the light output of the laser to ensure the absence of trial-to-trial and day-to-day variations in average light intensity for a given input setting.

Another part of the light output from the laser was polarized and attenuated sufficiently that photon-counting experiments could be performed by using an RCA Type 8575 photomultiplier tube, followed by a discriminator, amplifier, and pulse counter. In this way, the Poisson distribution of photons was measured directly.

Absolute photometric calibrations were made using an EG&G radiometer with a silicon photodiode at the front end, substituted in place of the subject's eye. These photocells are stable, providing an accurate measurement of the mean number of quanta at the cornea. Three subjects' switches were used to start the trial and to indicate yes and no responses. An electronic shutter was opened just before, and closed just after, the presentation of a stimulus to minimize the transmission of stray light to the subject. A computer recorded, on a trial-by-trial basis, the subject's response, the input voltage to the light modulator, the output of the photocell, and the output of the pulse counter.

B. Subjects

Subjects were four males ranging in age from 23 to 38 years. Subjects PRP and MEB wore corrective lenses during experimental sessions. Subject MEB was an experienced psychophysical observer; the others were not. All subjects appeared to have normal visual response under scotopic conditions as judged by the results of preliminary testing.

C. Subject Alignment

Subject alignment in the apparatus was maintained by the use of a dental-impression mouthbite. Initial alignment was achieved by using the following procedure. By previous adjustment, the target laser beam was made to pass through the focal point of the Maxwellian system that produced the fixation target. The position of this point in space was measured and marked by a piece of transparent plastic held in place by a clamp mounted on the wall. The plastic marker was used during alignment but removed during experimental sessions. The mouthbite was then adjusted to place the center of the subject's pupil at approximately the focal point marked on the plastic. Fine horizontal adjustment was then carried out by having the subject look to the left and to the right of fixation and mark the points at which the target beam disappeared. Since disappearance was caused by interception of the beam by the margin of the iris, equal left and right intervals ensured reasonable centering of the beam in the pupil. At the same time, a similar series of vertical adjustments was carried out. Before each experimental session, the fine-adjustment pro-

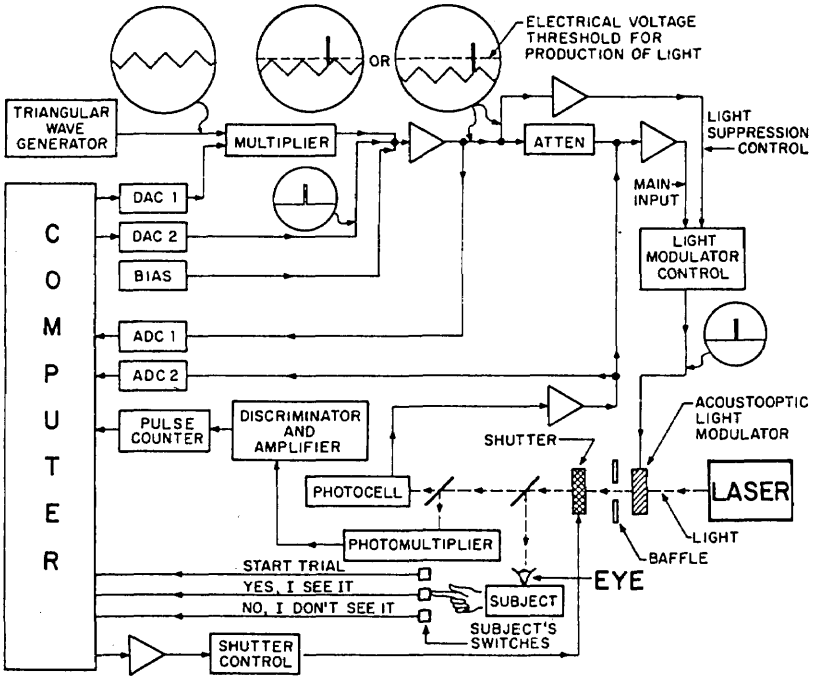

Fig. 1. Schematic representation of the experimental apparatus. The optical arrangement is illustrated in the lower portion of the figure.

cedure was used as a check on alignment. The need for subsequent adjustments was infrequent.

D. Presentation Format

A trial consisted of the presentation of a 1-msec flash of light, at the laser wavelength of 514.5 nm, or of a blank trial. A flash was chosen quasi-randomly from one of 10 mean energy levels, separated by 0.115 log unit, yielding a total range of about 1 log unit. A block of trials contained 5 trials at each mean level plus 10 blank trials, for a total of 60 trials. Subjects initiated a trial by pressing the start-trial switch. A trial followed the switch press by an interval of about 1 sec. Subjects were required to press either the yes or the no switch on each trial. The interstimulus interval was typically maintained at 3–5 sec. Time between blocks of trials averaged about 3–4 min and was governed by computer constraints.

E. Experimental Session

A session began with 35 min of dark adaptation interrupted only by two to four blocks of preliminary experimental trials. These dark-adaptation trials were used to allow the subject to become reacquainted with the task and to check for malfunctions. From 35 min in the dark until completion of the session, blocks of trials, alternating with the 3–4-min rest periods, were presented. An experimental session typically consisted of six blocks of trials and lasted from 1 to 1.5 h. Subjects knew the proportion of blank trials included in the presentation. They were allowed additional rest time if requested.

F. Preliminary Training

All subjects were allowed to gain familiarity with the task in preliminary sessions. During the training period, all subjects attempted to achieve a near-zero false-positive rate. To establish the range of mean intensities to be used in the main experiments, the upper limit of a set of intensities was established such that the subject always saw a light flash presented at this level. The subject was then instructed to report every flash seen in a session, being cautious not to report false positives. A subject was considered familiar with the task when he maintained a stable, low-false-positive rate while maintaining 100% frequency of seeing at an intensity level near his original maximum. Familiarity was typically obtained in two to five sessions.

For experimental sessions in which a high false-positive rate was required, subjects were simply asked to be more daring. They were asked still to report every flash that was seen and to respond negatively on trials in which nothing was seen. However, on trials in which a stimulus *might* have been present, subjects were encouraged to make positive responses without regard to the possibility of producing a false positive. In this way, false-positive rates ranging up to 33.3% were obtained. High false-positive rates (FPR's) were observed previously in a number of vision experiments.[11,12,15,18,20,21]

3. EXPERIMENTAL FREQUENCY-OF-SEEING CURVES WITH POISSON LIGHT

Frequency-of-seeing data generated by the four subjects (PRP, MEB, GV, and MCT) with low and high FPR's are presented as the filled circles in Figs. 2 and 3, respectively. The ordinate represents frequency of seeing on a linear scale (unity represents 100% frequency of seeing), and the abscissa represents, on a logarithmic scale, the average number of photons delivered to the cornea in the 1-msec flash, E, as photometrically measured with the radiometer. The open circle at the left in each set of data is the frequency of seeing for zero photons at the cornea and represents the experimental FPR, $\hat{P}_F$. The vertical bars surrounding each data point are the $\pm 1 - \sigma$ brackets, obtained by assuming that the trials at any given mean energy level are identical and independent,

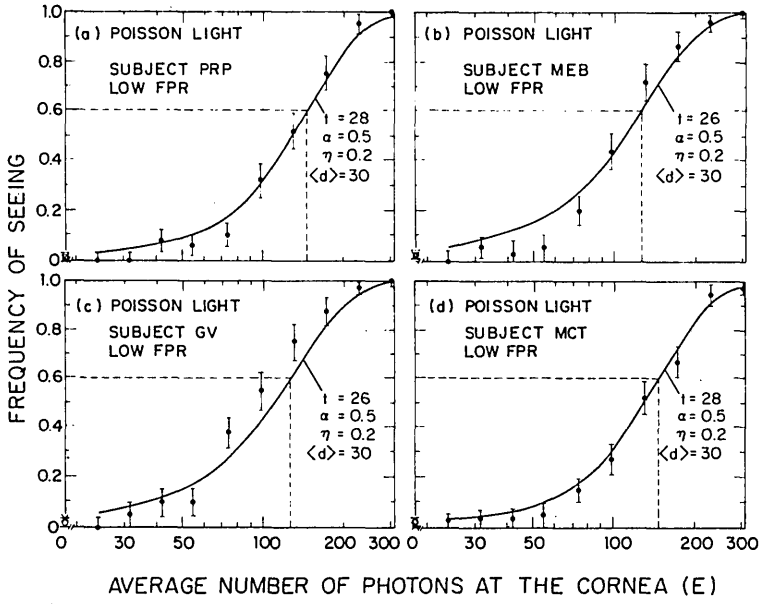

Fig. 2. Frequency-of-seeing data (filled circles) generated by the four subjects (PRP, MEB, GV, and MCT) with a Poisson light stimulus and low false-positive-rate conditions. The left-most open circle for each subject represents the experimental false-positive rate $\hat{P}_F$, and the vertical bars are the $\pm 1 - \sigma$ brackets discussed in the text. The dashed lines represent 60% frequency of seeing. The solid curves and crosses are theoretical probability-of-detection curves derived from a single family of summated NTA distributions ($\alpha = 0.5$, $\eta = 0.2$, $\langle d \rangle = 30$), with the best-fitting threshold value t specified in each quadrant of the figure (see Section 5 of text). Numerical values for the theoretical false-positive probability P_F and the experimental false-positive rate $\hat{P}_F$ (with error brackets), as well as the sum-of-squares goodness-of-fit measure, are presented in Table 1.

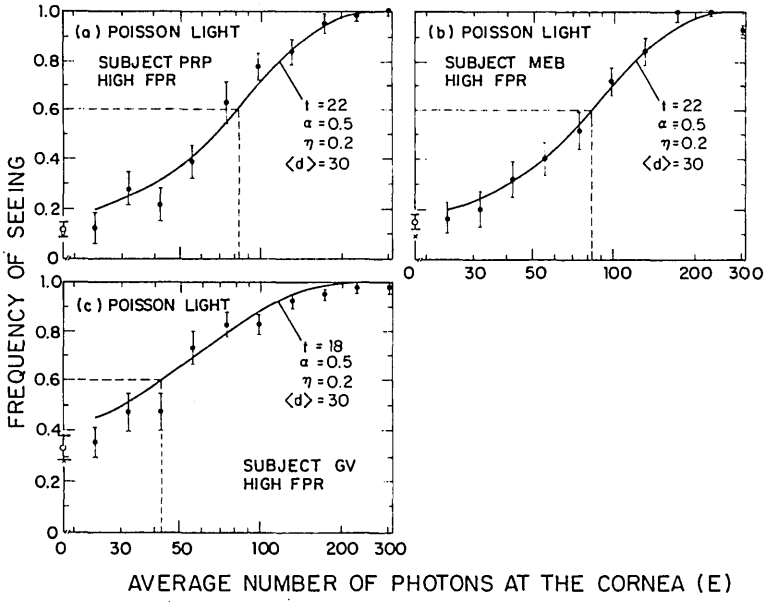

Fig. 3. Frequency-of-seeing data (filled circles) generated by three subjects (PRP, MEB, and GV) with a Poisson light stimulus and high false-positive-rate conditions. The left-most open circle for each subject represents the experimental false-positive rate $\hat{P}_F$, and the vertical bars are the $\pm 1 - \sigma$ brackets discussed in the text. The dashed lines represent 60% frequency of seeing. The solid curves and crosses are theoretical probability-of-detection curves derived from the same family of summated NTA distributions displayed in Fig. 2 ($\alpha = 0.5$, $\eta = 0.2$, $\langle d \rangle = 30$), with the best-fitting threshold value t specified in each quadrant of the figure (see Section 5 of text). Numerical values for the theoretical false-positive probability P_F and the experimental false-positive rate $\hat{P}_F$ (with error brackets), as well as the sum-of-squares goodness-of-fit measure, are presented in Table 1.

with two possible outcomes (each therefore represents a Bernoulli trial with constant probability of success). The error brackets must be considered as lower limits, however, because the data most often represented a combination of two different experimental sessions, and the condition of the subject can change from session to session.

The solid curves and crosses represent theoretical probability-of-detection and false-positive probabilities, respectively, and will be discussed in detail subsequently. For the moment, let us consider the solid curves to be empirical functions fitted to the frequency-of-seeing data. Then, from the low FPR data in Fig. 2, it is apparent that, for 60% fre-

quency of seeing (dashed lines), the average number of photons at the cornea lies between 127 and 147 for our four subjects. This is at the high end of the HSP range. Turning now to the high-FPR data in Fig. 3, the average number of photons is seen to lie between 42 and 82, which is at the low end of the HSP range. The low-FPR data go hand in hand with a high minimum-detectable average energy, whereas the high-FPR data are accompanied by a low minimum-detectable average energy.

It has long been known that sensitivity of detection and reliability of response are traded against each other[21,27]; from our experiments we see that this occurs over a broad range of both variables. In Section 5 we obtain a quantitative sensitivity-versus-reliability curve for our four subjects.

4. MODEL FOR THRESHOLD DETECTION

Every student of visual science knows that one of the principal conclusions drawn by HSP[1] was that the Poisson variability of the incident photon flux assumes a critical role in determining the shape of the psychometric function at threshold. The model constructed by these authors to explain their experimental results assumes that some number of photons, say, seven or so, is integrated together in the peripheral retina, in a narrow region of space and time, to send a message to higher centers in the brain that a stimulus had been detected. This is essentially a noiseless conception of visual detection (the false-positive probability is zero), in which the retina simply mirrors the Poisson fluctuations of the stimulus. The important parameter derived from the data in this model is the number of quanta required to be absorbed by the retina to elicit the sensation of seeing, t ($\simeq$5–8). The quantum efficiency of the visual process, η ($\simeq$5–10%), can be inferred from t and from a knowledge of the average number of photons at the cornea.

Although the version of the HSP model that usually comes to mind ignores all sources of fluctuations save those ascribable to the stimulus, HSP did allow for the qualitative introduction of a kind of central noise through "biological variability." After all, a variability in the threshold of the organism is associated with uncertainty or noise. (It will not provide a nonzero false-positive probability, however.)

Barlow's model[27] provided a concrete mechanism for dealing with nonzero false-positive reports and, at the same time, demonstrated that detectability and reliability could be viewed as being traded against each other. In addition to the parameters t and η, the average number of additive discrete noise events confusable with stimulus events, $\langle d \rangle$ ($\simeq$10), had to be included as a descriptive parameter ($\langle d \rangle$ is referred to the retina). Incorporating such additive noise makes good physiological sense because of the existence of the spontaneous neural discharge[35] (see Appendix A).

Multiplicative noise events are also important in the visual system at threshold. We argue in Appendix A that the Neyman Type-A (NTA) pulse-number distribution will satisfactorily represent the neural-counting distribution for such processes. This is the point of view taken by McGill.[28,29] More recently, Lillywhite[36] also emphasized the importance of multiplicative noise in visual information processing.

We proceed to translate these notions into a quantitative model for the processing carried out by the visual system in an HSP-type task. It is designed to incorporate a variety of old and new experimental results: Poisson stimulus fluctuations, high photometric quantum efficiency, central-processing loss, additive noise suggested by the spontaneous retinal discharge, multiplicative noise exemplified by the clustering of neural spikes at the retinal ganglion cell, and single-threshold processing.[37,38] The predictions of the model turn out to be quite consistent with our experimental frequency-of-seeing data, even when only a single parameter of the model is permitted to vary.

The block diagram of the model is presented in Fig. 4. We begin with a number of preliminary comments about the light source, which consists of a Poisson photon generator, a shutter, and an optional light modulator. A discussion of the modulated radiation, which is represented by the upper light path in Fig. 4, is deferred until Part 3 of this set of papers.[32] The Poisson photon generator, gated by the shutter, produces bursts of photons describable by a simple nonstationary, homogeneous Poisson point process (lower light path, denoted by PP), which gives rise to the well-known Poisson counting distribution

$$p(j|E) = E^j e^{-E}/j!. \tag{1a}$$

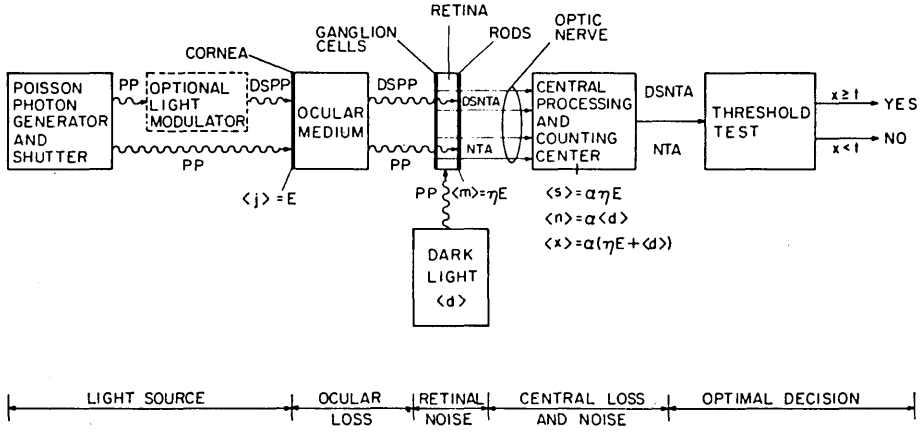

Fig. 4. Block diagram of model for visual system processing at threshold. The lower light path excludes the optional light modulator. For $\alpha \to 0$, with $\langle s \rangle$, $\langle n \rangle$, and $\langle x \rangle$ fixed, the model becomes identical with that proposed by Barlow[27]; for $\langle d \rangle \to 0$, with α and $\langle s \rangle$ as parameters, the model is equivalent to that presented by McGill[28,29]; whereas for $\langle d \rangle \to 0$ and $\alpha \to 0$, with $\langle s \rangle$ and $\langle x \rangle$ fixed, the model reduces to that presented by HSP.[1] A discussion of the upper light path is considered in Part 3 of this set of papers.[32]

Here $p(j|E)$ represents the probability of finding j photons in the stimulus duration T at the cornea when the integrated intensity (energy) E is fixed. The quantity $E = IAT$, where I is the light irradiance (intensity) and A is the (uniformly) illuminated area. The mean number of photons at the cornea $\langle j \rangle = E$, as is evident from inspection of Eq. (1a).

The light pulse incident upon the cornea traverses the ocular medium and the retina, undergoing loss through absorption and scattering, and is absorbed by the rods. In our case, the quantum efficiency η is defined as the fraction of photons incident upon the cornea that survive the passage and actually contribute to the activation of the rods; we refer to this as the ocular quantum efficiency. The best current photometric estimate for this quantum efficiency in humans, calculated by Barlow,[30] lies between 0.11 and 0.33. In spite of the absorption and scattering in the intervening medium, the statistics of the photons absorbed by the rods remain Poisson; the loss simply reduces the mean. At the retina, the number of photons m registered in time T is therefore described by the Poisson distribution

$$p(m|\eta E) = (\eta E)^m e^{-\eta E}/m!. \tag{1b}$$

Clearly, the mean number of photons per flash $\langle m \rangle = \eta E$. Equation (1b) provides an appropriate statistical description for the detection of most kinds of light used in vision experiments, including the dc-excited ribbon-filament tungsten lamp used by HSP and the (unmodulated) multimode Ar^+ laser used in our experiments.[39]

Following the reasoning presented in Appendix A, we now use the NTA distribution, a relatively simple counting distribution associated with a clustered point process, to describe the statistical character of the individual events at the output of our central-processing and -counting center in darkness and at low light levels. Most simply, we may conceive of this distribution as arising from a Poisson stimulus distribution of mean W, $p(m|W)$, associated with the signal or dark light, driving an independent Poisson neural-counting distribution associated with the retinal and central signal, $p(z|m)$. Since any number of stimulus events m may occur, and since all values of m contribute to the neural count, we sum over this variable.

The NTA distribution is written as[28,40,41]

$$p(z|W) = \sum_{m=0}^{\infty} p(z|m)p(m|W) = \sum_{m=0}^{\infty} \frac{(\alpha m)^z e^{-\alpha m}}{z!} \frac{W^m e^{-W}}{m!}, \tag{2a}$$

$$p(0|W) = \exp[W(e^{-\alpha} - 1)], \tag{2b}$$

with $W > 0$. The noise distribution is obtained by setting $z = n$ and $W = \langle d \rangle$, where $\langle d \rangle$ is the average Poisson dark-noise count (referred to the retina) in an integration time. The signal distribution emerges when $z = s$ and $W = \eta E$ (see Fig. 4). The signal-plus-noise distribution is the discrete convolution of the independent signal and noise distributions. The multiplication parameter α (>0) provides a measure of the average number of neural spikes per effective (light or dark) photon, assuming that the entire discharge cluster (which will have duration $\tau_p \sim$ 50–70 msec for light pulses that are of <32-msec duration; see Appendix A) is included in the central-counting interval T_c. We have set $\alpha = 0.5$ to provide results in accord with the estimated photometric quantum efficiency and with the estimated central efficiency (~50%) reported by Barlow[30,42] (see Appendix B). Since $\alpha < 1$, the effects of such NTA multiplied-Poisson noise are manifested as a decrease in the average count rate (this is designated as central loss in Fig. 4) and a concomitant increase in the observed variance-to-mean ratio (designated as central noise in Fig. 4). We will see subsequently that the character of our results does not depend on the precise value of α.

The mean, variance, and variance-to-mean ratio for the NTA distribution are, respectively,[41]

$$\langle z \rangle = \alpha W, \tag{3a}$$

$$\langle (\Delta z)^2 \rangle = (1 + \alpha)\alpha W, \tag{3b}$$

$$\langle (\Delta z)^2 \rangle / \langle z \rangle = 1 + \alpha. \tag{3c}$$

Note that the variance is proportional to the mean, so that the noise looks like excess shot noise.[43] The variance-to-mean ratio is always greater than unity, whereas this ratio is always precisely unity for the Poisson distribution. This indicates that the multiplication of the signal always introduces excess shot noise. Some years ago, Grimm[44] compiled tables of the cumulative density function for various values of $\langle z \rangle$ and α. The typical shapes that the distribution takes on are illustrated in Fig. 1 of the paper by Teich.[41] It is important to note that the NTA approaches the Gaussian as a limiting form[41] since many models for visual detection postulate a Gaussian internal variable.[6]

Finally, the output of the central-processing and -counting center is subjected to a likelihood-ratio test, which comprises an optimal processing strategy in the framework of signal detection theory.[10–12,15,16] Recently, Prucnal and Teich showed that, under a broad range of conditions, the likelihood-ratio test for the classical binary-decision problem reduces to a simple comparison of the number of counts with a single threshold.[38] This is a useful result in the context of visual information processing, as we emphasized previously.[37] It means that, to achieve optimal processing, the observer need not tabulate the results of repeated trials to accumulate signal and noise relative-frequency histograms and then carry out a complex calculation of the likelihood ratio.

Four parameters appear in our model: t, η, $\langle d \rangle$, and α. In mathematical terms, the detection problem is formulated as follows. At the counting center, the total number of noise events registered in the central-counting interval T_c is represented by an NTA discrete random variable n, with probability density function $p_N(n|\langle d \rangle)$, since the dark light at the retina is assumed to be Poisson with mean $\langle d \rangle$. Thus the noise mean at the counting center $\langle n \rangle = \alpha \langle d \rangle$ (see Fig. 4). For the values of $\langle n \rangle$ and α that we will encounter, $\log [p_N(n|\langle d \rangle)]$ will exhibit no point of inflection, so that single-threshold processing will be optimal.[38] The total number of signal events at the counting center, in the central-counting interval T_c, is similarly represented by a NTA discrete random variable s with probability density function $p_S(s|\eta E)$. The average number of photons at the cornea is E, so that the average number of photons activating rods in the retina is $\langle m \rangle = \eta E$, and the signal mean at the counting center is $\langle s \rangle = \alpha \langle m \rangle = \alpha \eta E$ (see Fig. 4). If the noise and signal random variables are additive, independent, and noninterfering, then whatever their individual statistical character, the total number of signal-plus-noise events registered at the central-

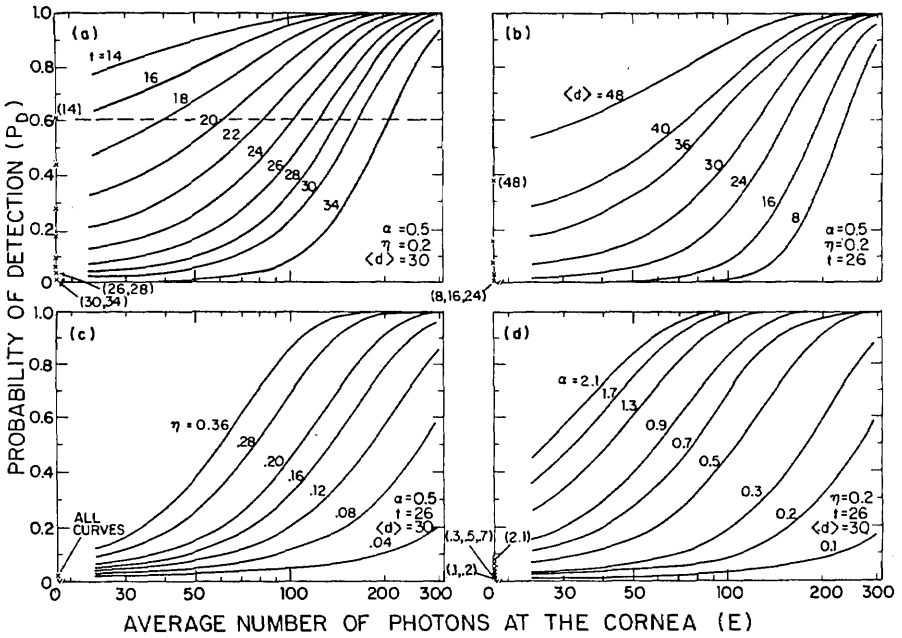

Fig. 5. (a) Theoretical probability of detection P_D (derived from summated NTA distributions) versus average number of photons at the cornea, E, with the threshold count t as a parameter. The multiplication parameter $\alpha = 0.5$, the quantum efficiency $\eta = 0.2$, and the retinal dark-light mean $\langle d \rangle = 30$. (b) $\alpha = 0.5$, $\eta = 0.2$, $t = 26$, and $\langle d \rangle$ as a parameter. (c) $\alpha = 0.5$, $t = 26$, $\langle d \rangle = 30$, and η as a parameter. (d) $\eta = 0.2$, $t = 26$, $\langle d \rangle = 30$, and α as a parameter.

counting center, in the interval T_c, is represented by a discrete random variable x, with probability density function $p_{SN}(x|\langle d \rangle, \eta E)$ given by

$$p_{SN}(x|\langle d \rangle, \eta E) = p_N(n|\langle d \rangle) * p_S(s|\eta E). \tag{4}$$

The symbol $*$ represents discrete convolution.

The theoretical false-positive probability P_F represents the probability that the noise count n is greater than, or equal to, the threshold t, i.e.,[16]

$$P_F = \sum_{n=t}^{\infty} p_N(n|\langle d \rangle). \tag{5}$$

The theoretical probability of detection P_D represents the probability that the signal-plus-noise count x is greater than, or equal to, the threshold t, i.e.,[16]

$$P_D(E) = \sum_{x=t}^{\infty} p_{SN}(x|\langle d \rangle, \eta E). \tag{6}$$

In the model considered by Barlow,[27] both the noise $p_N(n)$ and the signal $p_S(s)$ are Poisson. Since the convolution of two Poisson distributions remains Poisson, the signal-plus-noise distribution in that case is

$$p_{SN}(x) = \langle x \rangle^x e^{-\langle x \rangle}/x!, \tag{7}$$

and the theoretical probability-of-detection curves are, in accordance with Eq. (6), obtained from summated Poisson distributions. The convolution of two NTA distributions, with identical multiplication parameters α, can be similarly shown to remain NTA with parameter α.[40,41] Thus the signal-plus-noise distribution for the model considered here is described by Eq. (2) with $z = x$ and $W = (\eta E + \langle d \rangle)$. From Eq. (3), the mean and variance of the signal-plus-noise count are $\langle x \rangle = \alpha(\eta E + \langle d \rangle)$ and $\langle (\Delta x)^2 \rangle = (1 + \alpha)\alpha(\eta E + \langle d \rangle)$, respectively (see Fig. 4). The theoretical probability-of-detection curves (P_D versus E) are, in accordance with Eq. (6), obtained from summated NTA distributions. The receiver-operating characteristic (ROC) is obtained from Eqs. (5) and (6).

In Fig. 5, we present computer-generated families of such theoretical probability-of-detection curves versus the average number of photons at the cornea, E. In each quadrant of the figure, one of the parameters that enters our model is varied parametrically while the remaining parameters are kept constant. Thus in Fig. 5(a) we fix $\alpha = 0.5$, $\eta = 0.2$, and $\langle d \rangle = 30$ (we have chosen these values for reasons explained in Appendix B). In this set of curves, the threshold count t is varied parametrically; in Section 5 we will make use of Fig. 5(a) in fitting the experimental frequency-of-seeing curves reported earlier. The crosses at the left-hand boundary of the figure (zero photons at the cornea) represent the false-positive probabilities P_F for each of the 10 curves.

In Fig. 5(b), parameters are fixed at $\alpha = 0.5$, $\eta = 0.2$, and $t = 26$, and $\langle d \rangle$ is varied parametrically. Comparing Figs. 5(a) and 5(b), it is clear that increasing $\langle d \rangle$ has an effect on P_D similar to that of decreasing t, i.e., the curves become increasingly shallow. In Fig. 5(c), η is varied, with $\alpha = 0.5$, $t = 26$, and $\langle d \rangle = 30$. The P_D curves appear primarily to translate to the left with increasing η; the false-positive probability P_F depends only on α, t, and $\langle d \rangle$ and is independent of η [see Eq. (5)]. Finally, in Fig. 5(d), α is varied with $\eta = 0.2$, $t = 26$, and again $\langle d \rangle = 30$; the curves for increasing α and increasing η behave somewhat similarly, as expected, althouth P_F does depend on α. The dependence of the probability-of-detection curves, and the associated false-positive probabilities, on each of the parameters in our model is thus explicitly demonstrated in Fig. 5. ROC curves could be presented in the same way. In Section 5 we use this model to fit our experimental frequency-of-seeing curves for Poisson light.

5. EXTRACTION OF MODEL PARAMETERS FROM FREQUENCY-OF-SEEING DATA

There are many approaches that can be employed in attempting to fit to the frequency-of-seeing data the theoretical probability-of-detection curves generated by our model. The simplest approach, perhaps, is to fix all parameters at constant values, save the threshold count t, which we permit to vary parametrically. There then results a family of one-parameter probability-of-detection curves, such as that shown in Fig. 5(a), with each curve representing a different value of t. Using this method, we were able to fit, reasonably satisfactorily, all seven sets of frequency-of-seeing data presented in Figs. 2 and 3 (for both low and high FPR's). The particular family of curves illustrated in Fig. 5(a) ($\alpha = 0.5$, $\eta = 0.2$, $\langle d \rangle = 30$) was used in this procedure. The solid curves and crosses in Figs. 2 and 3 all belong to this theoretical family, with best-fitting threshold values ranging between $t = 18$ and $t = 28$, as specified in the figures and in Table 1. Also presented in Table 1 are the theoretical false-positive probability P_F and the experimental FPR $\hat{P}_F$ (with $\pm 1 - \sigma$ error brackets) for each curve. These are as consistent as can be expected, given the magnitude of the error brackets. The column containing the sum of squares in Table 1 provides a measure of the goodness of fit of the theory to the experimental data.

Our quick success with this elementary approach simply illustrates that there is at least one sensible set of average parameters (α, η, $\langle d \rangle$) that, when plugged into our model, provides a theory that is reasonably consistent with the data from all the subjects. Although we do not believe that these parameters are truly the same for all subjects, this assumption has provided us with a point of departure without getting us into trouble (as it likely would if our data were more accurate).

We next proceeded to fit each of the seven sets of data in Figs. 2 and 3 individually by means of a slightly different one-parameter procedure in which α and η were fixed at 0.5 and 0.2, respectively, while $\langle d \rangle$ and t were simultaneously adjusted both to match the theoretical and experimental false-positive rates (P_F and $\hat{P}_F$) and to minimize the sum-of-squares measure of fit. The theoretical probability-of-detection curves in this case are derived from different families of summated NTA distributions. The results are illustrated in Table 2, where it can be seen that the best-fitting values of the threshold obtained by this method range between $t = 18$ and $t = 32$. These values are quite similar to those obtained

Table 1. One-Parameter (t) Collective Fit to All Seven Sets of (Poisson-Light) Frequency-of-Seeing Data with Theoretical Probability-of-Detection Curves Derived from a Single Family of Summated Neyman Type-A Distributions[a]

Subject/ Condition	Best-Fitting Threshold Count t	Theoretical False-Positive Probability P_F (%)	Experimental False-Positive Rate $\hat{P}_F$ (%)	Sum of Squares
PRP (low FPR)	28	1.0	1.0 ± 0.9	0.0154
MEB (low FPR)	26	2.2	2.2 ± 1.3	0.0451
GV (low FPR)	26	2.2	0.8 ± 0.8	0.0546
MCT (low FPR)	28	1.0	1.5 ± 1.1	0.0122
PRP (high FPR)	22	9.2	10.8 ± 2.8	0.0331
MEB (high FPR)	22	9.2	14.0 ± 3.2	0.0175
GV (high FPR)	18	28.0	33.3 ± 4.3	0.0435

[a] The threshold count t that provides the best fit is indicated in the second column, when the remaining parameters are fixed at $\alpha = 0.5$, $\eta = 0.2$, and $\langle d \rangle = 30$. These theoretical probability-of-detection curves are shown as the solid curves in Figs. 2 and 3. Also tabulated, in the third and fourth columns, respectively, are the theoretical false-positive probability P_F and the experimental false-positive rate $\hat{P}_F$ (with error brackets) as well as the sum-of-squares measure of fit of theory to experiment (fifth column). The theoretical false-positive probabilities are indicated by crosses on Figs. 2 and 3. The number of blank trials $b = 120$ for each set of data.

Table 2. Individual Fits to Each of the Seven Sets of (Poisson-Light) Frequency-of-Seeing Data[a]

Subject/ Condition	Best-Fitting Dark-Light Mean Count $\langle d \rangle$	Best-Fitting Threshold Count t	Theoretical False-Positive Probability P_F (%)	Experimental False-Positive Rate $\hat{P}_F$ (%)	Sum of Squares
PRP (low FPR)	32	29	1.1	1.0 ± 0.9	0.0176
MEB (low FPR)	32	27	2.5	2.2 ± 1.3	0.0498
GV (low FPR)	16	18	1.0	0.8 ± 0.8	0.0198
MCT (low FPR)	38	32	1.6	1.5 ± 1.1	0.0196
PRP (high FPR)	36	25	11.0	10.8 ± 2.8	0.0406
MEB (high FPR)	48	31	14.0	14.0 ± 3.2	0.0349
GV (high FPR)	56	31	34.0	33.3 ± 4.3	0.0407

[a] The values of the dark-light mean count $\langle d \rangle$ and the threshold t that provide the best fit for a given subject/condition are indicated in the second and third columns, when the remaining parameters are fixed at $\alpha = 0.5$ and $\eta = 0.2$. The theoretical false-positive probability P_F was constrained (in the fitting procedure) to be approximately equal to the experimental false-positive rate $\hat{P}_F$, as is apparent from the fourth and fifth columns. This method therefore also represents a one-parameter fit. Comparison of the sum-of-squares measure of fit of theory to experiment (sixth column) with the equivalent column in Table 1 (fifth column) demonstrates that the fits are about equally good. These theoretical curves are derived from different families of summated Neyman Type-A distributions and are not shown in Figs. 2 and 3. The number of blank trials $b = 120$ for each set of data.

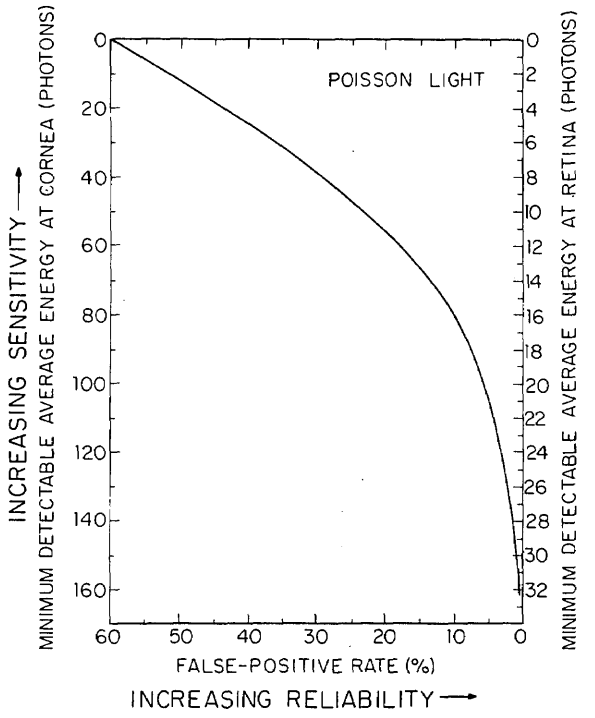

Fig. 6. Minimum-detectable average energy for 60% frequency of seeing of Poisson light (left ordinate, number of photons at the cornea; right ordinate, number of photons at the retina) versus false-positive rate (%) for four subjects. Sensitivity and reliability are traded against each other over a broad range. With an average of one photon at the retina, for example, 60% frequency of seeing is accompanied by a 55% false-positive rate. But with an average of 28 photons at the retina, 60% frequency of seeing is accompanied by a false-positive rate that is only about 1%. The curve was derived from the family of summated NTA distributions that was used to fit collectively all seven sets of (Poisson-light) frequency-of-seeing data [$\alpha = 0.5$, $\eta = 0.2$, $\langle d \rangle = 30$; see Figs. 2, 3, and 5(a) and Table 1]. It must be kept in mind that our experimental data extend only to a 33% FPR, however (see text). A personal curve for each subject could be obtained if longer experimental sessions could be conducted without fatiguing the subject.

by the first procedure. The sum of squares for the two procedures (fifth column of Table 1 and sixth column of Table 2) are also comparable, indicating that nothing is seriously awry. We could, of course, attempt to provide a two- and even a three-parameter fit to each data set separately in an effort to extract model parameters for individual subjects under specified conditions. But it appears to us that this level of effort is not warranted by the limited accuracy of our data, and we are quite satisfied with these simple, but consistent, one-parameter fits. In Part 2 of this set of papers,[31] we use the normalizing transform and probit analysis to provide an improved estimation procedure.

Having demonstrated that the shapes and behavior of the probability-of-detection curves presented in Fig. 5(a) are sensible, we now cast the results in a somewhat different form, to elucidate the trade-off between sensitivity and reliability of response. The horizontal dashed line at the 60% probability-of-detection level, together with the associated crosses on the left ordinate of Fig. 5(a), immediately allows us to provide a quantitative measure of the minimum-detectable average number of photons at the cornea versus the false-positive rate for our four subjects, as shown in Fig. 6. Sensitivity and reliability are traded against each other over a broad range. With an average of five photons at the cornea, for example, 60% frequency of seeing is accompanied by a 55% false-positive rate. But with an average of 140 photons at the cornea, 60% frequency of seeing is accompanied by a false-positive rate that is only about 1%. We must keep in mind, however, that our experimental data extended only to a 33% FPR. The validity of the extrapolation beyond this point is based on the assumption that the set of probability-of-detection curves presented in Fig. 5(a) is representative of frequency-of-seeing data for $t < 18$.

Furthermore, insofar as we accept the 20% model-dependent value for the ocular quantum efficiency η (admittedly this is a rough estimate), we can translate our minimum corneal energies into minimum retinal energies. The right ordinate of Fig. 6 illustrates this. Improved estimates of the model parameters would permit us to construct a personal sensitivity-reliability curve for each subject.

We have also been able to fit the experimental frequency-of-seeing data presented in Figs. 2 and 3 with theoretical probability-of-detection curves derived from Barlow's model,[27] in which both the signal and noise are Poisson, as well as with theoretical P_D curves derived from a variation of this model, in which the signal is NTA and the noise is Poisson. Using a three-parameter fitting procedure to minimize the sum of squares, we obtained excellent fits to the data in both cases, but the model parameters associated with the best-fitting curves are highly variable and appear to show no regular pattern. The associated theoretical false-positive probabilities, furthermore, are almost always smaller than the experimental FPR's. We have interpreted this as indicating that the effective noise in the visual system near threshold should properly be represented by a counting distribution with a variance greater than that of the Poisson.[45] The NTA is just such a distribution.

It is evident from the foregoing that theoretical probability-of-detection curves derived from summated NTA distributions do a good job of fitting experimental frequency-of-seeing data and provide model parameters of reasonable values under a broad range of false-positive rates.[46] But it is also evident that the frequency-of-seeing paradigm does not appear to permit the kind of precision that will allow the experimenter to discriminate sensitively among related alternative models. There are many ways in which probability-of-detection curves with virtually identical shapes can be generated, and one cannot conclude from the shape of these curves alone that the nature of the process has been determined. Nor will classical frequency-of-seeing data permit the extraction of more than approximate values of the relevant physiological parameters, even if it is known with certainty that a given model is the proper one. Variants of this procedure, in which data are collected at a small number of carefully chosen average energies, can be useful in this connection, however.[31]

6. CONCLUSION

Following the approach used by HSP in 1942, we collected calibrated frequency-of-seeing curves near the threshold of vision. Our experiments differed from theirs in that high false-report rates were encouraged in certain blocks of trials. A quantitative relationship between the average number of photons required at the cornea, for 60% frequency of seeing,

and the FPR demonstrates that sensitivity and reliability are traded against each other over a broad range.

The statistical properties of various sources of noise at threshold (stimulus, retinal, and central) were distilled from a number of physical, neurophysiological, and psychophysical experiments. The overall noise has been categorized into two types: additive Poisson and multiplicative Poisson. A neural-counting model for threshold detection was developed. It incorporates a variety of old and new experimental and theoretical results: Poisson stimulus fluctuations, high photometric quantum efficiency, central-processing loss, additive noise suggested by the spontaneous retinal discharge, multiplicative noise exemplified by the clustering of neural spikes at the retinal ganglion cell, and single-threshold processing. The resulting probability-of-detection curves are derived from summated NTA distributions. Within the limitations of the paradigm, they are in accord with our frequency-of-seeing data for sensible values of the model parameters (dark-noise count, quantum and central efficiencies, and threshold count).

The internal neural-counting distribution is represented in our model by the NTA distribution, both in the dark and in response to a stimulus. This counting distribution, and indeed the entire class of counting distributions arising from multiplied and cascaded Poisson processes,[41,43,47–49] exhibits a count variance proportional to the count mean. Thus their fluctuation properties are manifested as excess shot noise[43]; they evidently bear a close relationship to the Poisson. This similarity appears in the limits of the distributions as well: the NTA is skewed at low levels, and it approaches the Gaussian at high levels.[41] The body of psychophysical and neurophysiological measurements that appear to require these particular characteristics of the Poisson can, therefore, be satisfied by the NTA distribution. In fact, a bit more latitude is available in the latter case, because the NTA has two free parameters rather than one. It is interesting that the outcome of Sakitt's threshold-rating experiments[21,50] can be interpreted as suggesting that the internal decision random variable is discrete and Gaussian-like, with a variance greater than the mean.[50] The NTA distribution fits this description well.

Because of the properties of this distribution, it immediately follows that our model gives rise to different increment and decrement thresholds,[51] that it can be coupled with probit analysis to provide improved threshold-parameter estimation,[31] and that it leads to the deVries–Rose intensity-discrimination law[52,53] at light levels that are low (but above the additive noise level).[28,29,36,54] We know that the retinal ganglion cell discharge measured by Barlow *et al.*[55] (for an on-center, brisk-sustained unit stimulated by short, small light stimuli) exhibits counting behavior describable by the NTA distribution (see Appendix A). Interestingly, under the same conditions, the intensity-discrimination behavior of such a cell is describable by the deVries–Rose law.[56,57] At higher levels of adaptation, the effects of saturation[58] and refractoriness[59–61] come into play. The NTA distribution is quite robust, however, and, under rather broad conditions, the refractoriness-modified counting distribution will remain NTA (the refractoriness will simply alter the variance-to-mean ratio).[62] Ultimately, however, the count variance will decrease below the count mean, and Weber's law will prevail.[63]

Finally we note that, aside from the range of physiological data with which our model is consistent, it consists of only a single channel. As such, it is inherently simpler than multiple-channel models.[17–19] In short, the effects of neural noise can be subtly made to join the effects of Poisson stimulus fluctuations, leaving many important results intact. The role of non-Poisson stimulus fluctuations can also be established in the framework of such a model, as is considered in Part 3 of this set of papers.[32]

Appendix A. Neurophysiological Evidence for Additive and Multiplicative Noise in the Visual System

In 1971, Barlow *et al.*[55] conducted an important series of experiments on the neural discharge in the retinal ganglion cell of the cat. For a number of on-center cells, they demonstrated that the neural pulse-number distribution (PND), both in darkness and in response to brief but dim flashes of light, exhibited a variance in excess of the mean. Thus the spike discharge could not be understood in terms of a Poisson process, even if additive Poisson noise were included. They presented a possible anatomical explanation for these observations in terms of multiple pathways in the retina from the rod to the ganglion cell, both for photons and for dark light. Indeed, Baylor and Yau and their collaborators[64,65] have convincingly shown that the response of vertebrate rod outer segments to single photons and to dark photons[66,67] takes the form of smooth current pulses (of about 1-pA magnitude) that reflect the underlying Poisson excitations. But whatever the mechanism, the observation of a neural-count variance in excess of the count mean reveals that the neural spikes form a clustered point process and that the fluctuation characteristics of the incident Poisson photons are not faithfully relayed by the retina. Support for this observation is provided in more recent data, at higher adaptation levels but still not far above threshold,[68] as well as in the study of Levick and Zacks.[69] The latter work demonstrated that, near threshold, the ganglion-cell spike response exhibits a time course with a minimum duration of 50–70 msec, no matter how brief the flash.

Barlow *et al.* showed that the mean and variance of the NTA counting distribution,[40,41] although they did not refer to it by name, adequately accounted for their experimental observations of these quantities. They were careful to demonstrate, however, that a number of different mathematical constructs would fit the data. We have recently shown[61] that the maintained-discharge interspike-interval histograms for one of their (on-center brisk-sustained) units could be modeled as a shot-noise-driven doubly stochastic Poisson point process (SNDP), modified somewhat by relative refractoriness. For a counting time T that is long in comparison with the linear-filter response time τ_p in the SNDP model, the expected pulse-number distribution turns out to be precisely the NTA.[41,43,47] This is true both for the stationary case (maintained discharge) and for the nonstationary case, in which the system is excited by a pulse of light, provided only that the duration of the pulse τ_s is short ($\tau_s \ll \tau_p + T$).[48] In the experiments of Barlow *et al.*,[55] $\tau_s = 10$ msec, $\tau_p \simeq 30$ msec, and $T = 200$ msec, so that this condition is well satisfied.

The NTA distribution has been considered before in the

context of visual neurophysiology.[70] It results from a multiplicative cascade of two Poisson distributions[41,43] but enjoys a generality that reaches beyond that description. Even in the presence of refractoriness or dead time, it often provides an appropriate description for the pulse-number distribution.[62] Indeed, we have been able to fit the PND data of Barlow *et al.*[55] for different luminance levels by using a convolution of two NTA distributions, one representing the dark–light discharge and the other representing the response to a flash of light of specified energy.[71] In short, additive Poisson noise, together with multiplicative Poisson noise, provides a good description for the discharge behavior in (at least some[72]) retinal ganglion cells at the threshold of vision.

The axons of the retinal ganglion cells comprising the optic nerve travel to central locations in the midbrain (superior colliculus) and thalamus [lateral geniculate nuclei (LGN)]. The signals continue on to the primary visual (striate) cortex. Fibers project from the visual cortex to associated cortical areas and back to the superior colliculus and to the lateral geniculate nuclei. The spontaneous interspike-interval histograms recorded at the LGN often appear to exhibit an excess of moderately short intervals relative to the exponential distribution.[73,74] This indicates spike clustering at the LGN, as observed in the ganglion cell and described by the SNDP.[61] It is tempting to conjecture that the combination of additive and multiplicative Poisson noise also provides a suitable description for the statistical behavior of the discharge at LGN cells in darkness and at low light levels.

In the current state of our knowledge, however, it is hopeless to attempt to detail, and to follow microscopically, the statistical character of the signal along its individual pathways. Instead, let us consider for a moment a k-stage cascade of Poisson point processes, each buffered by a linear filter. We have shown[49] that this produces a clustered output point process, for which the count variance remains proportional to the count mean.[75] This is true for both the stationary and nonstationary cases. We may wish to consider the information flux reaching the counting center as being carried on a parallel set of such channels. Çinlar[76] has shown that, under specified conditions, the superposition of a set of such component clustered point processes itself converges to a clustered point process. It seems that, once present, multiplication noise arising from clustering remains. This is true both for the dark discharge and for the response to light.

We therefore posit that the statistical distribution of neural events, on which a decision is based for the detection of a flash of light at threshold, is associated with a clustered (multiplied) point process. We use the NTA distribution to capture the essential statistical character of this clustering.

The mechanism can be viewed in a simplified way. McGill[28,29] argued that the smearing together of many neural paths at a hypothetical counting center in the chain to the visual cortex produces a Poisson-like central noise process under a broad range of conditions. There is ample mathematical support for such a convergence[76–78]; it basically requires independence and uniform sparseness for the individual channels. The Poisson flow of photons from the light source then modulates this Poisson central noise process, leading directly to the NTA counting distribution. This is seen to be a hybrid approach; it is in part stimulus based,[1,52,53] in part neural based.[6,7]

In whatever way we choose to view the information transfer in the visual system, it is not likely that the NTA counting distribution provides a perfect representation for our neural signal at the hypothetical counting center. Rather, it is a well-understood two-parameter distribution that captures the essence of the effects that we wish to represent: stimulus fluctuations (and additive dark–light fluctuations) and multiplicative neural noise.

Appendix B. Choice of Model Parameters

We briefly discuss our choice of model parameters. Barlow[30] has estimated that the photometric quantum efficiency η lies between 11 and 33% for the human. If the more recent results of Baylor *et al.*[65] for the "fraction exciting" in the toad are applicable, then this range contracts to 11–17%. We used $\eta = 20\%$ in our calculations, but the choice is not critical.

Barlow[42] also considers a central efficiency of 50% as a reasonable value to be expected. He sees this[30] as the most likely way of reconciling the 5.5% quantum efficiency from psychophysics[1] with the 11% lower limit of the photometric quantum efficiency. Based on this argument, we used $\alpha = 0.5$.

For the average dark count, we chose $\langle d \rangle = 30$, referred to the retina. This was obtained as follows. We used Østerberg's[79] figure of 1900 rods/0.0069 mm^2 at 17.5° eccentricity on the temporal retina. The receptive field size in the peripheral retina is not well known under scotopic conditions. However, extrapolating Wilson and Bergen's[80] data to the conditions of our experiment yields a representative value of 1° (0.088 mm^2). We also used the estimate of Baylor *et al.*[67] of 0.008 isomerizations/sec/rod for the human, and a temporal integration time of 0.2 sec. Combining all these estimates yields 38 isomerizations/summation area/summation time, close to our value $\langle d \rangle = 30$. An estimate not too different from this can also be inferred from the retinal-ganglion-cell dark discharge.[61]

We note that our probit estimates of all these parameters[31] lie in the same range.

ACKNOWLEDGMENTS

The authors are grateful to the National Science Foundation and to the National Institutes of Health for support of this work.

* Present address, Bell Laboratories, Holmdel, New Jersey 07733.

† Present address, Department of Visual Physiology, Wills Eye Hospital, Philadelphia, Pennsylvania 19107.

‡ Present address, Department of Psychology, University of California at San Diego, La Jolla, California 92093.

REFERENCES

1. S. Hecht, S. Shlaer, and M. H. Pirenne, "Energy, quanta, and vision," J. Gen. Physiol. **25**, 819–840 (1942).
2. S. P. Langley, "Energy and vision," Philos. Mag. Ser. 5, **27**, 1–23 (1889).
3. H. A. van der Velden, "Over het aantal lichtquanta, dat nodig is voor een lichtprikkel bij het menselijk oog," Physica **11**, 179–189 (1944); "The number of quanta necessary for the perception of light of the human eye," Ophthalmologica **111**, 321–331 (1946) [translation].

4. M. A. Bouman and H. A. van der Velden, "The two-quanta explanation of the dependences of the threshold values and visual acuity on the visual angle and the time of observation," J. Opt. Soc. Am. **37**, 908–919 (1947).
5. E. Baumgardt, "The quantic and statistical basis of visual excitation," J. Gen. Physiol. **31**, 269–290 (1950).
6. H. R. Blackwell, "Neural theories of simple visual discriminations," J. Opt. Soc. Am. **53**, 129–160 (1963).
7. W. J. Crozier, "On the sensory discrimination of intensities," Proc. Nat. Acad. Sci. U.S.A. **22**, 412–416 (1936).
8. S. Hecht, "Energy and vision." in *Science In Progress*, A Baitsell, ed. (Yale U. Press, New Haven, Conn., 1945), pp. 75–95, 309–310.
9. E. J. Denton and M. H. Pirenne, "The absolute sensitivity and functional stability of the human eye," J. Physiol. **123**, 417–442 (1954).
10. W. W. Peterson, T. G. Birdsall, and W. C. Fox, "The theory of signal detectability," IRE Trans. Prof. Group Inf. Theory **PGIT-4**, 171–212 (1954).
11. W. P. Tanner, Jr., and J. A. Swets, "The human use of information—I. Signal detection for the case of the signal known exactly," IRE Trans. Prof. Group Inf. Theory **PGIT-4**, 213–221 (1954).
12. W. P. Tanner, Jr., and J. A. Swets, "A decision-making theory of visual detection," Psychol. Rev. **61**, 401–409 (1954).
13. M. Treisman, "Noise and Weber's law: the discrimination of brightness and other dimensions," Psychol. Rev. **71**, 314–330 (1964).
14. M. Treisman, "A statistical decision model for sensory discrimination which predicts Weber's law and other sensory laws: some results of a computer simulation," Percept. Psychophys. **1**, 203–230 (1966).
15. D. M. Green and J. A. Swets, *Signal Detection Theory and Psychophysics* (Wiley, New York, 1966) (reprinted by Krieger, Huntington, N.Y., 1974).
16. H. L. van Trees, *Detection, Estimation and Modulation Theory—Part I* (Wiley, New York, 1968).
17. G. S. Brindley, "The relation of frequency of detection to intensity of a stimulus for a system of many independent detectors each of which is stimulated by a m-quantum coincidence," J. Physiol. **169**, 412–415 (1963).
18. J. Nachmias and E. C. Kocher, "Detection and discrimination of luminance increments," J. Opt. Soc. Am. **60**, 382–389 (1970).
19. T. E. Cohn, L. N. Thibos, and R. N. Kleinstein, "Detection of a luminance increment," J. Opt. Soc. Am. **64**, 1321–1327 (1974); T. E. Cohn and D. J. Lasley, "Detectability of a luminance increment: Effect of spatial uncertainty," J. Opt. Soc. Am. **64**, 1715–1719 (1974).
20. J. Nachmias and R. M. Steinman, "Study of absolute visual detection by the rating-scale method," J. Opt. Soc. Am. **53**, 1206–1213 (1963).
21. B. Sakitt, "Counting every quantum," J. Physiol. **223**, 131–150 (1972).
22. M. A. Bouman, "History and present status of quantum theory in vision," in *Sensory Communication*, W. Rosenblith, ed. (MIT Press, Cambridge, Mass., 1961), Chap. 21, pp. 377–401.
23. M. A. Bouman and J. J. Koenderink, "Psychophysical basis of coincidence mechanisms in the human visual system," in *Reviews of Physiology: Biochemistry and Experimental Pharmacology* (Springer-Verlag, Berlin, 1972), Vol. 65, pp. 125–172.
24. E. Baumgardt, "Threshold quantal problems," in *Handbook of Sensory Physiology: Visual Psychophysics*, D. Jameson and L. M. Hurvich, eds. (Springer-Verlag, Berlin, 1972), Vol. VII/4, Chap. 2, pp. 29–55.
25. J. Nachmias, "Signal detection theory and its application to problems in vision," in *Handbook of Sensory Physiology: Visual Psychophysics*, D. Jameson and L. M. Hurvich, eds. (Springer-Verlag, Berlin, 1972), Vol. VII/4, Chap. 3, pp. 56–77.
26. G. Buchsbaum, "The retina as a two-dimensional detector array in the context of color vision theories and signal detection theory," Proc. IEEE **69**, 772–786 (1981).
27. H. B. Barlow, "Retinal noise and absolute threshold," J. Opt. Soc. Am. **46**, 634–639 (1956).
28. W. J. McGill, "Neural counting mechanisms and energy detection in audition," J. Math. Psychol. **4**, 351–376 (1967).
29. W. J. McGill, "Poisson counting and detection in sensory systems," in *Concepts of Communications: Interpersonal, Intrapersonal, and Mathematical*, E. F. Beckenbach and C. B. Tompkins, eds. (Wiley, New York, 1971), Chap. 9, pp. 257–281.
30. H. B. Barlow, "Retinal and central factors in human vision limited by noise," in *Photoreception in Vertebrates*, H. B. Barlow and P. Fatt, eds. (Academic, New York, 1977), Chap. 19, pp. 337–358.
31. P.R. Prucnal and M. C. Teich, "Multiplication noise in the human visual system at threshold: 2. Probit estimation of parameters," Biol. Cybern. **43**, 87–96 (1982).
32. M. C. Teich, P. R. Prucnal, G. Vannucci, M. E. Breton, and W. J. McGill, "Multiplication noise in the human visual system at threshold: 3. The role of non-Poisson quantum fluctuations," Biol. Cybern. (submitted for publication).
33. M. C. Teich, P. R. Prucnal, G. Vannucci, M. E. Breton and W. J. McGill, "Role of quantum fluctuations and the Neyman Type-A distribution in human vision," J. Opt. Soc. Am. **69**, 1469(A) (1979).
34. M. E. Breton, M. C. Teich, and L. Matin, "Intensity fluctuations produced by multimode lasers in combination with dielectric beamsplitters," Behavioral Res. Methods Instrum. **9**, 324–325 (1977).
35. S. W. Kuffler, R. FitzHugh, and H. B. Barlow, "Maintained activity in the cat's retina in light and darkness," J. Gen. Physiol. **40**, 683–702 (1957).
36. P. G. Lillywhite, "Multiplicative intrinsic noise and the limits to visual performance," Vision Res. **21**, 291–296 (1981).
37. M. C. Teich, P. R. Prucnal, and G. Vannucci, "Optimum photon detection with a simple counting processor," Opt. Lett. **1**, 208–210 (1977).
38. P. R. Prucnal and M. C. Teich, "Single-threshold detection of a random signal in noise with multiple independent observations: 1. Discrete case with application to optical communications," Appl. Opt. **17**, 3576–3583 (1978).
39. The Poisson nature of the detected photons follows directly from the small value of the degeneracy parameter of the light, $\delta = \langle m \rangle \tau_c / T$, where τ_c is the coherence time of the light [see L. Mandel, Proc. Phys. Soc. **74**, 233–242 (1959); B. E. A. Saleh, *Photoelectron Statistics* (Springer-Verlag, Berlin, 1978)]. For the source used by HSP, $\langle m \rangle \simeq 10$, $T \simeq 10^{-3}$ sec, and $\tau_c \simeq 10^{-13}$ sec, whereas for our multimode Ar^+ laser source $\tau_c \simeq 10^{-9}$ sec [see G. Vannucci and M. C. Teich, Appl. Opt. **19**, 548–553 (1980)]. In both cases $\delta \ll 1$. We shall see in Part 3 of this series[32] that certain rather common sources of visible radiation, such as television and oscilloscope images produced by cathodoluminescence, as well as image-intensified light [see A. van Meeteren, Vision Res. **18**, 257–267 (1978)], in general, generate non-Poisson photon statistics [see Refs. 43 and 47]. Their use in vision experiments therefore requires exceptional care.
40. J. Neyman, "On a new class of 'contagious' distributions, applicable in entomology and bacteriology," Ann. Math. Stat. **10**, 35–57 (1939).
41. M. C. Teich, "Role of the doubly stochastic Neyman Type-A and Thomas counting distributions in photon detection," Appl. Opt. **20**, 2457–2467 (1981).
42. H. B. Barlow, "The absolute efficiency of perceptual decisions," Phil. Trans. R. Soc. Lond. Ser. B **290**, 71–82 (1980); A. F. Burgess, R. F. Wagner, R. J. Jennings, and H. B. Barlow "Efficiency of human visual signal discrimination," Science **214**, 93–94 (1981).
43. M. C. Teich and B. E. A. Saleh, "Fluctuation properties of multiplied-Poisson light: Measurement of the photon-counting distribution for radioluminescence radiation from glass," Phys. Rev. A **24**, 1651–1654 (1981).
44. H. Grimm, "Tafeln der Neyman-Verteilung Typ-A," Biom. Z. **6**, 10–23 (1964).
45. M. C. Teich, P. R. Prucnal, G. Vannucci, M. E. Breton, and W. J. McGill, "Non-Poisson nature of the effective noise in the visual system near threshold," J. Opt. Soc. Am. **68**, 1454(A) (1978).
46. Several of our stipulations on the format of detection are, no doubt, unnecessarily restrictive. For example, the assumptions of a single counting focus and a fixed integration time could likely be relaxed without seriously affecting the outcome.
47. B. E. A. Saleh and M. C. Teich, "Multiplied-Poisson noise in

pulse, particle, and photon detection," Proc. IEEE, **70** (to be published, 1982).
48. B. E. A. Saleh and M. C. Teich, "Statistical properties of a nonstationary Neyman-Scott cluster process," IEEE Trans. Inf. Theory (submitted for publication).
49. K. Matsuo, B. E. A. Saleh, and M. C. Teich, "Cascaded Poisson processes," J. Stat. Phys. (submitted for publication).
50. B. Sakitt, "Canonical ratings," Percept. Psychophys. **6,** 478–488 (1974).
51. T. E. Cohn, "A new hypothesis to explain why the increment threshold exceeds the decrement threshold," Vision Res. **14,** 1277–1279 (1974).
52. A. Rose, "The relative sensitivities of television pick-up tubes, photographic film, and the human eye," Proc. IRE **30,** 293–300 (1942).
53. Hl. de Vries, "The quantum character of light and its bearing upon the threshold of vision, the differential sensitivity and acuity of the eye," Physica **10,** 553–564 (1943).
54. P. R. Prucnal and M. C. Teich, "An increment threshold law for stimuli of arbitrary statistics," J. Math. Psychol. **21,** 168–177 (1980).
55. H. B. Barlow, W. R. Levick, and M. Yoon, "Responses to single quanta of light in retinal ganglion cells of the cat," Vision Res. **11,** Suppl. 3, 87–101 (1971).
56. H. B. Barlow and W. R. Levick, "Threshold setting by the surround of cat retinal ganglion cells," J. Physiol. **259,** 737–757 (1976).
57. P. Lennie, "Scotopic increment thresholds in retinal ganglion cells," Vision Res. **19,** 425–430 (1979).
58. Y. Y. Zeevi and S. S. Mangoubi, "Noise suppression in photoreceptors and its relevance to incremental intensity thresholds," J. Opt. Soc. Am. **68,** 1772–1776 (1978).
59. M. C. Teich, L. Matin, and B. I. Cantor, "Refractoriness in the maintained discharge of the cat's retinal ganglion cell," J. Opt. Soc. Am. **68,** 386–402 (1978).
60. M. C. Teich and P. Diament, "Relative refractoriness in visual information processing," Biol. Cybern. **38,** 187–191 (1980).
61. M. C. Teich and B. E. A. Saleh, "Interevent-time statistics for shot-noise-driven self-exciting point processes in photon detection," J. Opt. Soc. Am. **71,** 771–776 (1981).
62. B. E. A. Saleh, J. Tavolacci, and M. C. Teich, "Discrimination of shot-noise-driven Poisson processes by external dead time: application to radioluminescence from glass," IEEE J. Quantum Electron. **QE-17,** 2341–2350 (1981).
63. H. A. van der Velden, "Quanteuse verschijnselen bij het zien," Ned. Tijdschr. Natuurkd. **15,** 147–151 (1949).
64. K.-W. Yau, T. D. Lamb, and D. A. Baylor, "Light-induced fluctuations in membrane current of single toad rod outer segments," Nature **269,** 78–80 (1977).
65. D. A. Baylor, T. D. Lamb, and K.-W. Yau, "Responses of retinal rods to single photons," J. Physiol. **288,** 613–634 (1979).
66. K.-W. Yau, G. Matthews, and D. A. Baylor, "Thermal activation of the visual transduction mechanism in retinal rods," Nature **279,** 785–786 (1979).
67. D. A. Baylor, G. Matthews, and K.-W. Yau, "Two components of electrical dark noise in toad retinal rod outer segments," J. Physiol. **309,** 591–621 (1980).
68. H. B. Barlow, T. E. Cohn (School of Optometry; University of California, Berkeley; Calif. 94720), W. R. Levick, and L. N. Thibos, "Low light level performance of cat retinal ganglion cells" (personal communication).
69. W. R. Levick and J. L. Zacks, "Responses of cat retinal ganglion cells to brief flashes of light," J. Physiol. **206,** 677–700 (1970).
70. S. Yeandle and J. B. Spiegler, "Light evoked and spontaneous discrete waves in the ventral nerve photoreceptor of *Limulus*," J. Gen. Physiol. **61,** 552–571 (1973).
71. We are grateful to H. B. Barlow and W. R. Levick for providing us with experimental data.
72. W. R. Levick, "Form and function of cat retinal ganglion cells," Nature **254,** 659–662 (1975).
73. P. O. Bishop, W. R. Levick, and W. O. Williams, "Statistical analysis of the dark discharge of lateral geniculate neurones," J. Physiol. **170,** 598–612 (1964).
74. H. Nakahama, N. Ishii, M. Yamamoto, and H. Saito, "Stochastic properties of spontaneous impulse activity in central single neurons," Tohoku J. Exp. Med. **104,** 373–409 (1971).
75. If we assume that the counting time is very large in comparison with the decay times τ_p for all k stages, and that the multiplication parameter of each stage is given by α_j, the variance-to-mean ratio is[49]

$$R = \langle(\Delta n)^2\rangle/\langle n\rangle = 1 + \sum_{i=1}^{k-1}\left(\prod_{j=i}^{k-1}\alpha_j\right) \equiv 1 + \rho.$$

This is the origin of the quantity ρ used in Part 2 of this series of papers.[31] If the multiplication parameters of all stages are identical, and equal to α, then

$$R = 1 + \alpha[(1 - \alpha^{k-1})/(1 - \alpha)]$$

and

$$\rho = \alpha[(1 - \alpha^{k-1})/(1 - \alpha)].$$

For $k = 1$ and $k = 2$, we recover the usual expressions for the Poisson and Neyman Type-A distributions, respectively. Random deletion from an SNDP also maintains the cluster property of this process, although with a reduction in the multiplication parameter α.[47]
76. E. Çinlar, "Superposition of point processes," in *Stochastic Point Processes: Statistical Analysis, Theory and Applications*, P. A. W. Lewis, ed. (Wiley-Interscience, New York, 1972), pp. 549–606.
77. D. R. Cox and W. L. Smith, "The superposition of several strictly periodic sequences of events," Biometrika **40,** 1–11 (1953).
78. D. R. Cox and W. L. Smith, "On the superposition of renewal processes," Biometrika **41,** 91–99 (1954).
79. G. Østerberg, "Topography of the layer of rods and cones in the human retina," Acta Ophthalmol. Suppl. **6,** 1–103 (1935).
80. H. R. Wilson and J. R. Bergen, "A four mechanism model for threshold spatial vision," Vision Res. **19,** 19–32 (1979).